energies

Article

Parameter Optimization of Drilling Cuttings Entering into Sieve Holes on a Surface Multi-Hole (SMH) Drill Pipe

Lipei Ding [1], Yuning Sun [1,2,*], Zhiming Wang [1,*], Weibin Song [1,2] and Yonglong Wang [1]

[1] School of Energy Science and Engineering, Henan Polytechnic University, Jiaozuo 454000, China; dinglphpu@163.com (L.D.); swb@hpu.edu.cn (W.S.); wylong@hpu.edu.cn (Y.W.)
[2] Collaborative Innovation Center of Coal Work Safety, Jiaozuo 454000, China
* Correspondence: sunyn@hpu.edu.cn (Y.S.); quiet_wong@hpu.edu.cn (Z.W.)

Abstract: The borehole drilling distance is short in soft and gas outburst-prone coal seams because of drill pipe jamming induced by cuttings accumulating in the borehole, hindering coal mine gas hazard prevention and utilization. A surface multi-hole (SMH) drill pipe composed of a bearing layer, fluid layer, and anti-sparking layer was proposed preliminarily, where several sieve holes were also set. To study the process of drilling cuttings in boreholes entering into the inner hole of an SMH drill pipe and its influencing factors, mechanical model analysis, CFD-DEM simulation, and a physical experiment were conducted. Our research results show the cutting entering region (CER) of the SMH drill pipe shrinks with the rotary speed, expands with the external extrusion force, and is offset with the sieve hole inclination angle. The drilling cuttings migrate and accumulate over time between the borehole wall and SMH drill pipe, which increases their compressive forces and induces increases in the mass and diameter of those entering into the sieve holes. The sieve hole diameter and depth are critical factors impacting the drilling cuttings entering into the sieve holes, which is also related to an appropriate rotary speed of the drill pipe. Finally, SMH drill pipes with a sieve hole diameter of 10 mm, inclination angle of 10°, and depth of 8 mm were determined and trial-manufactured.

Keywords: borehole drilling; surface multi-hole drill pipe; sieve hole; cutting entering region

Citation: Ding, L.; Sun, Y.; Wang, Z.; Song, W.; Wang, Y. Parameter Optimization of Drilling Cuttings Entering into Sieve Holes on a Surface Multi-Hole (SMH) Drill Pipe. *Energies* **2022**, *15*, 3763. https://doi.org/10.3390/en15103763

Academic Editor: Vamegh Rasouli

Received: 18 April 2022
Accepted: 16 May 2022
Published: 20 May 2022

1. Introduction

Coal is an important natural resource for industry production and human life throughout the world [1,2]. For the major coal producers, such as China, India, Australia, the USA, etc., coal seam gas extraction and utilization are critical to the safety of coal mines, as well as to reducing the greenhouse gases emitted into the atmosphere [3,4]. Generally, methane stored in coal seams can be extracted via boreholes under negative suction pressure, which has been studied for many years [5–7]. For coal seams with high strength and low gas content, it is feasible to conduct borehole drilling in the coal seam by conventional drilling techniques. However, there are many soft and outburst-prone coal seams in the provinces of Henan, Anhui, Guizhou, Shanxi, etc., in China, where the borehole length in the coal seam is very short and cannot meet the requirement of coal seam gas efficient extraction [8–10]. Therefore, it is urgent to develop novel drill pipes to improve the borehole length in soft and outburst-prone coal seams and clarify their drilling cutting discharge mechanisms.

Figure 1 shows the conventional drill pipes adopted in coal seam borehole excavation. The spiral blade drill pipe (Figure 1a) and smooth-surfaced drill pipe (Figure 1b) were adopted in coal seam borehole drilling in China during the 20th century and are still used now. The smooth-surfaced drill pipe's rotary motion helps to disperse the drilling cuttings into the main flow region and, hence, improves the quality of drilling cutting transport and borehole cleaning [11–14]. Because of the complexity of coal seam geology, the drilling length of the spiral blade and smooth-surfaced drill pipes only range from about 30 to 70 m in soft and gas outburst-prone coal seams. The borehole along the coal seam tends to

become damaged and cracked due to its low strength and high gas content [9,15]. Based on the elasticity–plasticity theory, the coal around the in-seam borehole can be divided into three typical regions, including stress relaxation, stress concentration, and intact stress regions. During borehole drilling in the coal and gas outburst-prone coal seam, the coal in the stress relaxation and concentration regions tends to flow and crack, inducing a large amount of gas–coal outburst from the borehole wall and the jamming of drill pipes [16,17]. Sun Y. et al. analyzed the reasons for drilling difficulty in the soft coal seam and proposed a concept of a "drilling cave" (Figure 1f), which is formed around an in-seam borehole under the effects of in situ stress, gas pressure, coal mechanical properties, and drilling disturbance. The velocity of airflow could decrease due to the large space of the drilling cave, which induces a large quantity of drilling cuttings to concentrate around drill pipes in the drilling cave, inducing serious drill pipe jamming. The blockage of the drilling cutting discharge channel outside the drill pipe was considered to be the primary cause of the drilling difficulties [18].

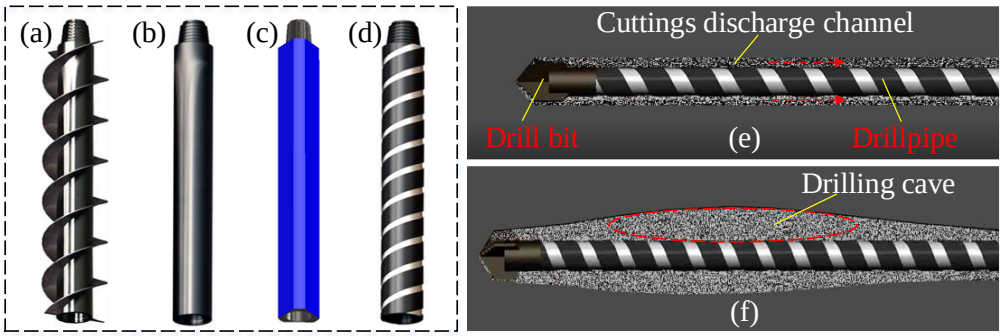

Figure 1. Drilling techniques in soft and outburst-prone coal seam. (**a**) Spiral blade drill pipe; (**b**) smooth-surfaced drill pipe; (**c**) prismatic drill pipe; (**d**) grooved drill pipe; (**e**) normal drilling condition; and (**f**) drill pipe jamming.

Directional drilling technology has also been widely used in borehole drilling in coal seams, whose longest drilling length is about 3000 m in the coal seam with a firmness coefficient greater than 1.5 [19–22]. However, in coal and gas outburst-prone seams, the borehole length created by the directional drilling technology is no longer than that made by conventional rotary drilling technology, because the drill pipes of the directional drilling technology could be locked tightly by the coal from the cracked borehole, barely able to remove the drill pipes from the seam [23,24].

To solve the problem of drill pipe jamming in soft and gas outburst-prone coal seams, some novel drill pipes have been developed. As shown in Figure 1c, a prismatic drill pipe was proposed and successfully applied in the provinces of Henan, Shanxi, and other regions in China [25,26]. By a numerical simulation method, the interaction of drilling fluid and prismatic drill pipe rotation was analyzed. It showed that a fluid vortex would form on the surface of the prismatic drill pipe during the rotation, which was beneficial for drill cuttings' migration into the borehole and reduced the probability of drill pipe jamming [27,28]. Sun, Y. et al. proposed a novel grooved drill pipe, which is shown Figure 1d. Using the grooved drill pipe, drilling cuttings in the drilling cave could be discharged easily by the drag forces of fluid and the interactions of the grooves' rotation [18,29,30]. However, with an increase in mining depth, the in situ stress in the seam increases fast, which induces a jamming risk for the grooved drill pipe. The stability of a borehole can be improved by spraying foam concrete onto the borehole wall during drilling, but the operation process is very complex, causing the drilling efficiency to be low [31].

For the smooth-surfaced, prismatic, grooved drill pipes, and directional drill pipes, drilling cutting migration is between the hole wall and drill pipe (as shown in Figure 1e), which is critical for borehole drilling and is influenced by fluid velocity, drill pipe structure, rotary speed of drill pipe, etc. [32]. Under high in situ stress, borehole deformation is inevitable, which causes an increase in compressive force imposed on the surface of the

drill pipes, locking the drill pipe [10]. Therefore, drilling cutting transportation between the borehole wall and drill pipes is unreliable for long-distance borehole drilling in soft and gas outburst-prone coal seams. This could cause borehole blockage and drill pipe jamming [33,34].

As shown in Table 1, most of the drilling technology and drilling cutting migration studies have been based on the conventional drill pipes introduced above, but the difficult problems of drilling in soft and gas outburst-prone coal seams, such as borehole blockage, drill pipe jamming, etc., have still not been resolved.

Table 1. Analysis methods for a drill pipe's working mechanism and drill pipes' advantages and disadvantages.

Type of Drill Pipes	Analysis Methods	Advantages	Disadvantages
Spiral blade drill pipe	Theoretical and mechanical analysis; multiphase flow in CFD; CFD-DEM	Cuttings discharged by spiral blade, no need for fluid.	Rotation resistance is large; drill pipe jams easily.
Smooth-surfaced drill pipe		Structure of drill pipe is simple. The drill pipe strength is high.	Borehole blockage easy in soft coal seam.
Prismatic drill pipe		Vortex release effect on cuttings in borehole.	Drillpipe joint strength is low; drillpipe jamming.
Grooved drill pipe		Cuttings discharged by fluid and spiral grooves.	The spiral delivery function is small; borehole blockage in soft coal seam.

Therefore, we proposed a novel surface multi-hole (SMH) drill pipe with a different structure and working mechanism from the conventional drill pipes, by which the drilling cuttings could enter into the inner hole of the SMH drill pipe through sieve holes and then be transported out of the borehole by fluid. The drilling cutting transport channel of the SMH drill pipe is located in the center of drill pipe and is not affected by borehole stability. In addition, after the drilling cuttings enter into the SMH drill pipe via the sieve holes, the drill pipe's rotation resistance decreases, which is crucial for long-distance borehole drilling in the soft and gas outburst-prone coal seam. However, there is little research on this novel SMH drill pipe. In this paper, we focus on the process of the drilling cuttings entering into the sieve holes on the SMH drill pipe, the influencing factors, and the parameter optimization of the SMH drill pipe, which contributes to illuminating the working mechanism of the SMH drill pipe and obtaining the optimal parameters. Furthermore, the SMH drill pipe proposed in this study provides a new method for long-distance borehole drilling in soft and gas outburst-prone coal seam, supporting gas hazard prevention and unconventional natural gas utilization.

2. SMH Drill Pipe and Mechanical Model of Drilling Cuttings Entering into the Sieve Holes

2.1. SMH Drill Pipe

As shown in Figure 2a, the SMH drill pipe is composed of a bearing layer, fluid layer, and anti-sparking layer. On the surface of the bearing layer, there are several axial and spiral grooves. In the fluid layer, there are four fluid channels. The inner hole of the anti-sparking layer is for discharging drilling cuttings. Additionally, for all three layers, there are several sieve holes from the axial grooves to the inner hole. The sieve holes are not connected to the fluid channels. Drilling cuttings produced from the bottom of the borehole and the wall of the borehole can enter into the inner hole of the anti-sparking layer via the sieve holes. Then, drilling cuttings in the inner hole can be discharged out of the borehole under the drag force of air/water flow, which is critical to borehole drilling for the SMH drill pipe in soft and outburst-prone coal seams.

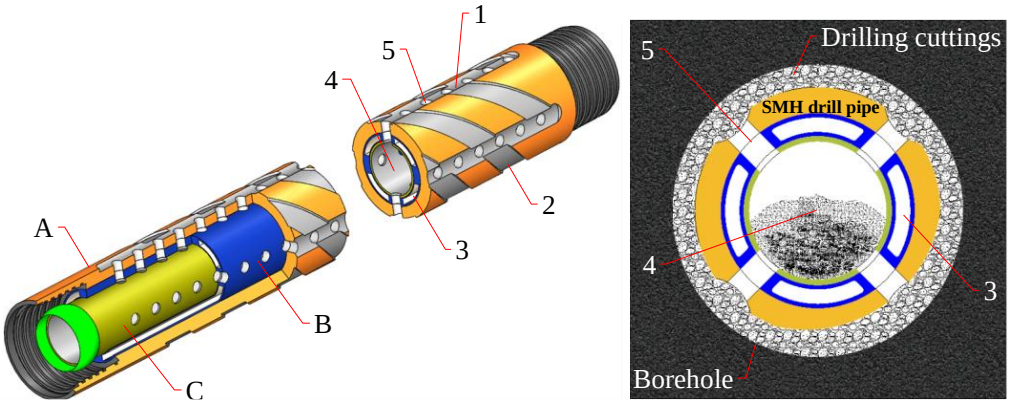

(**a**) (**b**)

Figure 2. Structure of SMH drill pipe. (**a**) Three-dimensional structure; (**b**) cross section of SMH drill pipe in borehole. A. Bearing layer; B. fluid layer; C. anti-sparking layer. 1. Axial grooves; 2. spiral grooves; 3. fluid channel; 4. inner hole; 5. sieve hole.

2.2. Mechanical Model of Drilling Cuttings Entering into the Sieve Holes

Taking horizontal drilling as an example, the forces imposed on a single drilling cutting at the sieve hole of the SMH drill pipe are shown in Figure 3. It can be seen that the forces imposed on the drilling cutting are composed of gravity, friction force, supporting force, and external extrusion force. The necessary condition for drilling cuttings entering into the sieve holes of the SMH drill pipe is that the radial resultant force is greater than the centrifugal force, i.e., $F_r > F_c$ [35].

$$F_r = F_e + \mathrm{Mg}\,[\sin\theta + \cos(\theta - \beta)(u\cos\beta - \sin\beta)] \quad (1)$$

$$F_c = \mathrm{Mr}\pi^2 n^2/900 \quad (2)$$

where F_r and F_c represent the radial resultant force and centrifugal force imposed on the drilling cuttings, respectively; F_e is the external extrusion force on the drilling cutting, pointing towards the center of the drill pipe; M is the average mass of the drilling cutting; and g is the gravitational acceleration, 9.8 m^2/s in this paper. θ is the angle between OA and OB; β is the angle between the sieve hole axis and OA, i.e., the inclination angle of the sieve holes; u is the friction coefficient between the drilling cutting and the sieve hole wall; r is the distance from the drilling cuttings to the inner hole axis; and n is the rotary speed of the SMH drill pipe.

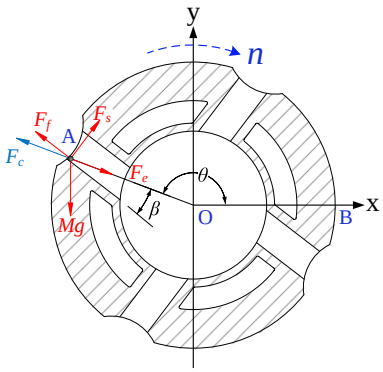

Figure 3. Mechanical model of drilling cuttings entering into the sieve holes of an SMH drill pipe.

In order to explain the mechanical characteristics of drilling cuttings entering into the sieve holes preliminarily, we calculated the radial resultant force of a single drilling cutting particle and compared it with the centrifugal force. Through experimentation, we assumed

that a drilling cutting has an average mass of 0.05 g, the outer diameter of the SMH drill pipe is 89 mm, the inner hole diameter is 49 mm, and the sieve hole diameter is 10 mm.

In this study, we defined the angle range of $F_r > F_c$ in the drill pipe cross section as the concept of a cutting entry region (CER). When the sieve hole inclination angle is 10°, and the external extrusion force is 1.5×10^{-4} N, the resulting relation plots of F_r and F_c are shown in Figure 4a. From this, we can see that only a region of the circumference direction of the SMH drill pipe is the CER. When the sieve holes are in the CER, drilling cuttings can enter into the sieve holes. On the contrary, when the sieve holes are outside the CER, the drilling cuttings cannot enter into the sieve holes. As shown in Figure 4b, the higher the rotary speed of the drill pipe, the greater the centrifugal force imposed on the drilling cuttings in the sieve holes, and the smaller the range of the CER. As shown in Figure 4c, when the sieve hole is set to an inclined one, biasing the rotary direction of the drill pipe as shown in Figure 3, the position of the CER is offset toward the reverse direction of the drill pipe rotation, but this has little effect on the size of the CER. As shown in Figure 4d, when the drilling cuttings are subjected to external extrusion forces of different sizes, the CER also changes. The greater the extrusion force is, the greater the resultant force of cuttings entering is, and the greater the CER is, correspondingly. The increase in CER is beneficial for the drilling cuttings entering into the sieve holes.

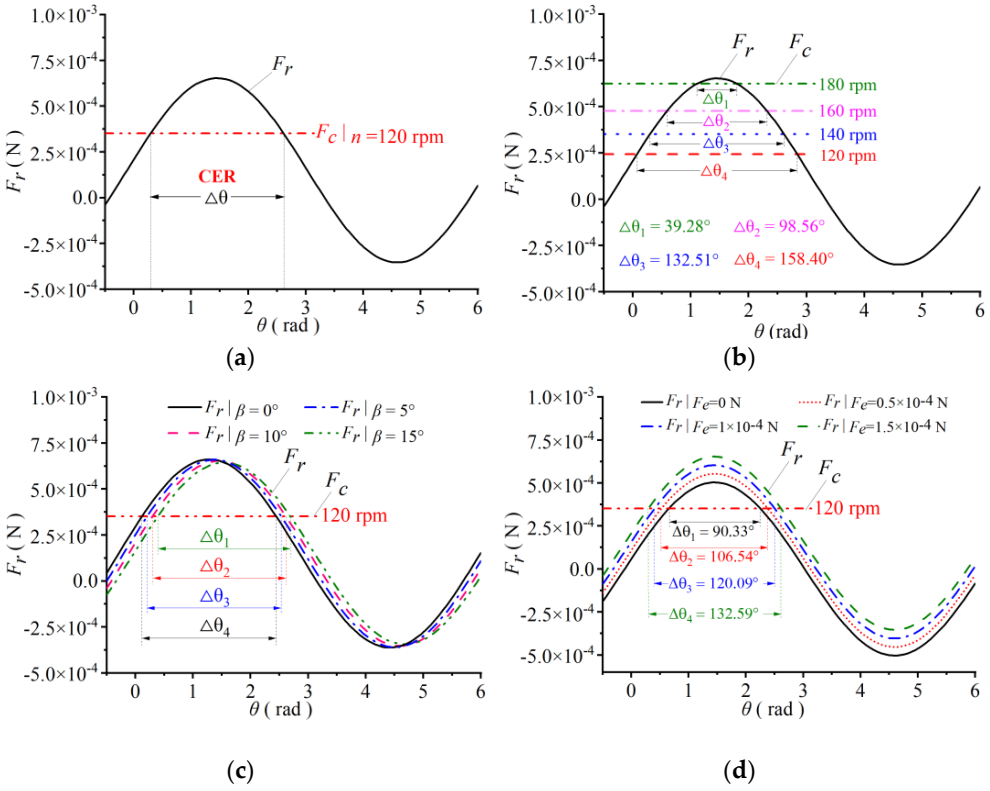

Figure 4. Mechanical analysis diagram. (**a**) F_r and F_c variations with θ at a rotary speed of 120 rpm, a β value of 10°, and an extrusion force of 1.5×10^{-4} N; (**b**) F_r and F_c variations with θ at a β value of 10°, an extrusion force of 1.5×10^{-4} N, and rotary speeds of 120, 140, 160, and 180 rpm; (**c**) F_r and F_c variations with θ at a rotary speed of 120 rpm, an extrusion force of 1.5×10^{-4} N, and β values of 0°, 5°, 10°, and 15°; (**d**) F_r and F_c variations with θ at a rotary speed of 120 rpm, a β value of 10°, and an extrusion force of 0, 0.5×10^{-4}, 1.0×10^{-4}, and 1.5×10^{-4} N.

The mechanical analysis only considered the influences of the rotary speed of the SMH drill pipe, sieve hole inclination angle, and external extrusion force on the entrance of the drilling cuttings into the sieve holes. However, there might be other factors affecting drilling, such as the sieve hole diameter, sieve hole depth, interaction between drilling cuttings, etc. Therefore, it was necessary to carry out numerical and physical simulations

to further explore the process and mechanism of drilling cuttings entering into the sieve holes, which is of importance to optimize the SMH drill pipe structure.

3. Numerical Simulation by CFD-DEM Method

3.1. Geometric Model and Boundary Conditions

As shown in Figure 2a, the fluid channels set in the bearing layer of the SMH drill pipe are used to convey water/air, which has little effect on the entrance of drilling cuttings into the sieve holes. Therefore, the fluid channels were omitted for simplification. Figure 5 shows the geometric model of the SMH drill pipe. The outer diameter of the SMH drill pipe was 89 mm, the inner hole diameter was 49 mm, and the borehole inner diameter was 110 mm. The length of the drill pipe was 1000 mm. By the CFD-DEM method, the drilling cuttings' migration process was simulated under drill pipe rotation and fluid (the fluid is air in this paper) drag. This numerical simulation was performed using FLUENT15.0 combined and coupled with EDEM2.7 [36–42]. As shown in Figure 5, Sections 1 and 2 were set on two ends of the model. Air entered into the model from Section 2 and flowed via the spaces between the borehole wall and drill pipe wall, the inner hole of the drill pipe, and the sieve holes. Drilling cuttings produced from the particle factory flowed to the outlet. It should be noticed that there was no air or drilling cutting migration by Section 1, since the inner hole of the SMH drill pipe is the only channel for drilling cutting discharge at the opening of borehole.

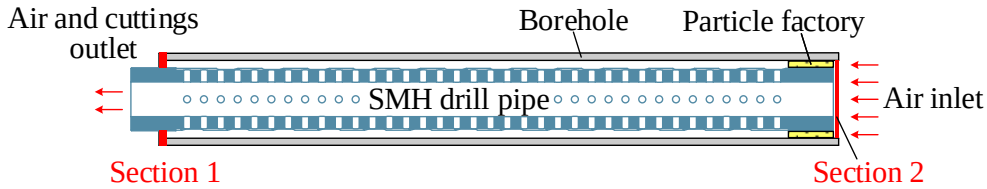

Figure 5. Geometric model of an SMH drill pipe in a borehole.

In the CFD modeling, the calculation domain of this study was the region inside the finite length borehole, and the borehole wall was stable without deformation. The unstructured mesh was adopted for the modeling, and the number of cells was 15,604. The air velocity inlet condition was given at Section 2, and the air velocity was 10 m/s. The pressure outlet condition was adopted for the outlet, and the pressure was set equal to 1 atm. The gravitational acceleration direction was vertical downward, and its value was 9.81 m/s^2. The selected turbulence model was the realizable *k*-*ε* turbulence model. The standard wall function approach was used near the wall. The CFD and DEM were coupled by the Eulerian–Eulerian method. To achieve a satisfactory convergence, the CFD and DEM time steps were set at 1×10^{-3} s and 1×10^{-5} s, respectively. The DEM time step was set 100 times smaller than the CFD time step [37,43].

Drilling cuttings were simplified as numerous particles in this section. Drilling cuttings from four coal mines in different regions of China were collected. Then, the drilling cuttings were divided into six groups, including 0~1 mm, 1~3 mm, 3~6 mm, 6~9 mm, 9~12 mm, and >12 mm. For the drilling cuttings from the four coal mines, the diameter distribution is shown in Figure 6. It can be seen that the diameter distributions of the drilling cuttings from different coal mines are different. Additionally, the lower the firmness coefficient of coal is, the larger the proportion of small size cuttings is. For soft coal seams, the proportion of drilling cuttings less than 3 mm is more than 50%.

A particle factory was set at one of the ends of the geometric model shown in Figure 5. Because the shapes of the drilling cuttings were irregular, the basic cutting particle in this simulation was composed of four 2 mm particles, and its effective size was $6 \times 5 \times 4$ mm. To analyze the larger particle size range, referring to the distribution characteristics of drilling cuttings in the soft coal seam (Figure 6), the sizes and mass percentages of the drilling cutting particles produced by the particle factory were 0.5 times (50%), 1 times (30%), and 1.5 times (20%) the size of the basic cutting particle.

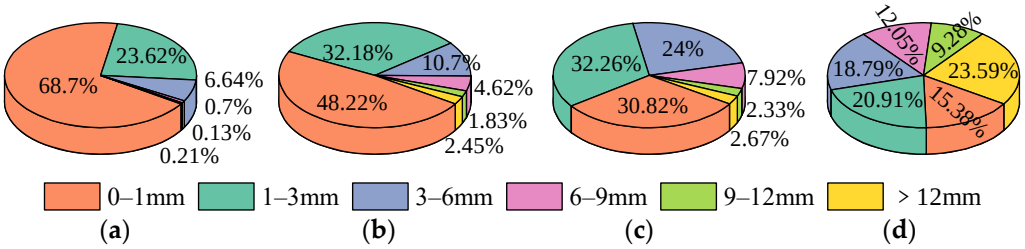

Figure 6. The diameter distributions of drilling cuttings from: (**a**) Shoushan coal mine; (**b**) Mengjin coal mine; (**c**) Pingdingshan 1# coal mine; and (**d**) Tunliu coal mine with firmness coefficients of 0.18–0.22, 0.12–0.46, 0.21–2.61, and 0.44–0.53, respectively.

3.2. Numerical Simulation Results

3.2.1. Drilling Cutting Migration

As shown in Figure 7, the drilling cuttings between the borehole wall and the SHM drill pipe gradually moved from Section 2 to Section 1 between 0.2 and 0.8 s. The drilling cutting migration was influenced by gravity, particle–particle interactions, particle–drill pipe interactions, and the drag force of the air flow. Figure 8 shows the distribution shape of the drilling cuttings on the surface of the SMH drill pipe at 0.8 s and the drilling cuttings' velocity vectors. It can be seen that drilling cuttings in the spiral groove had an axial velocity component V_t to the left. From Figures 7 and 8, it can be seen that the drilling cuttings were distributed along the spiral and axial grooves and migrated forward with the rotation of the SMH drill pipe, indicating that the grooves on the bearing layer of the SMH drill pipe helped the migration of drilling cuttings. The drilling cuttings accumulated near Section 1, which can be attributed to no particle or air flow in Section 1. Near Section 1, the number of accumulated drilling cuttings increased with time. Furthermore, there were more drilling cuttings entering into the inner hole of the SMH drill pipe with the increase in drilling cutting accumulation near Section 1.

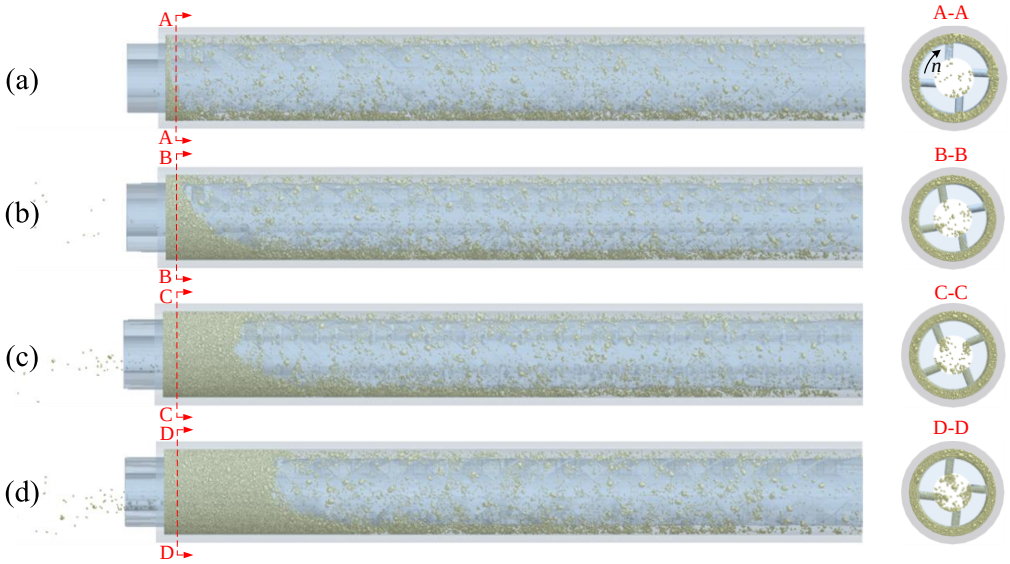

Figure 7. Drilling cutting migration at: (**a**) 0.2 s, (**b**) 0.4 s, (**c**) 0.6 s, and (**d**) 0.8 s.

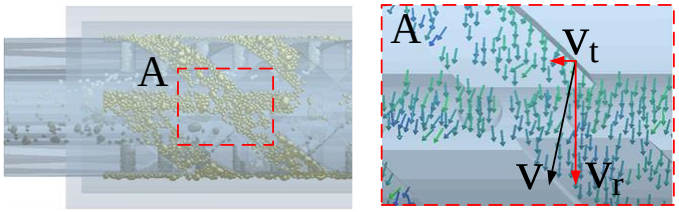

Figure 8. Drilling cutting distribution on grooves shape at 0.8 s and velocity vectors.

3.2.2. Compressive Forces and Velocities of Drilling Cuttings

The compressive forces of drilling cuttings in the borehole at 0.2 s, 0.4 s, 0.6 s, and 0.8 s are shown in Figure 9. It can be seen that there was little compressive force on the drilling cuttings at 0.2 s, whose maximum compressive force was only 0.35 N. At 0.4 s, there were more drilling cuttings accumulated near Section 1, inducing the increase in the compressive forces on the drilling cuttings, whose maximum value was 1.00 N. Additionally, at 0.6 s and 0.8 s, the numbers of drilling cuttings with the compressive force of 1.00 N were more than those at 0.2 s and 0.4 s.

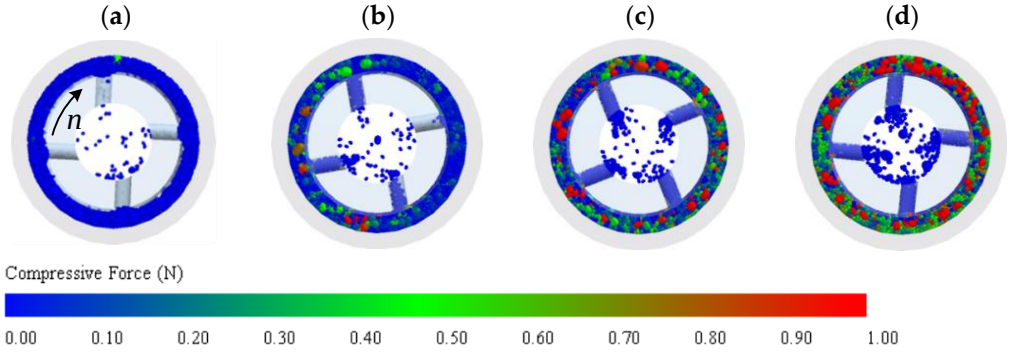

Figure 9. Compressive forces on drilling cuttings at: (**a**) 0.2 s; (**b**) 0.4 s; (**c**) 0.6 s, and (**d**) 0.8 s.

The drilling cuttings' average compressive forces out of the SMH drill pipe and the maximum diameter of drilling cuttings entering into the sieve holes are shown in Figure 10a. It can be seen that the average compressive forces of drilling cuttings out of the SMH drill pipe gradually increased over time. When the average compressive force was lower than 0.075 N, the maximum diameter of the drilling cuttings entering into the sieve holes was 6 mm. The maximum diameter of the drilling cuttings entering into the sieve holes increased with the increased average compression force. Figure 10b shows the total mass variation in drilling cuttings entering the sieve holes over time. Combining Figure 10a,b, it can be seen that the number of drilling cuttings entering into the sieve holes increased with the increase in the average values of the compressive forces on the drilling cuttings.

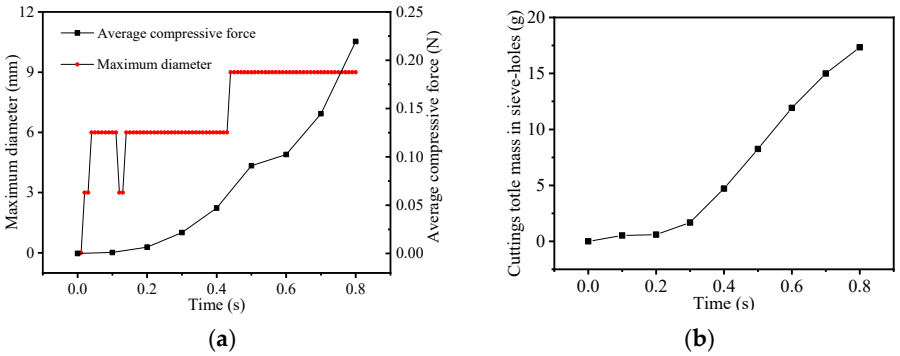

Figure 10. Average compressive force and total mass of drilling cutting variations over time. (**a**) Average compressive force of drilling cuttings outside the drill pipe and the maximum diameter of the drilling cuttings entering into the sieve holes; (**b**) Drilling cutting total mass in the sieve holes.

Figure 11 shows the drilling cuttings' velocity vectors' evolution over time. It can be seen that the velocities of the drilling cuttings at 0.2 s were about 2.00 m/s, indicating fast migration between the SMH drill pipe and the borehole wall. At 0.4 s, the velocities of the drilling cuttings at the bottom and left upper sections of the borehole were less than 0.6 m/s, but the velocities of the drilling cuttings at the right upper section were about 2.0 m/s. This indicates that drilling cuttings outside the drill pipe accumulated first in the bottom and left upper sections of the borehole under the action of gravity and drill rotation. Despite the SMH drill pipe rotation, the velocities of the drilling cuttings near Section 1 were about 0 at 0.6 s and 0.8 s, but the velocities of the drilling cuttings near the SMH drill pipe were about 0.6~1.2 m/s. This indicates that with the drilling cutting accumulation near Section 1, the compressive forces imposed on cuttings increased to inhibit their migration. However, the drilling cuttings on the surface of the SHM drill pipe could migrate with the interaction of the drilling cuttings and the drill pipe.

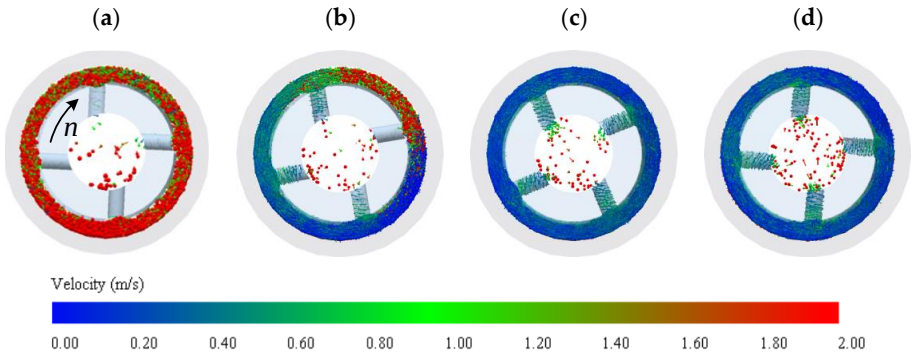

Figure 11. Drilling cutting velocities at: (**a**) 0.2 s, (**b**) 0.4 s, (**c**) 0.6 s, and (**d**) 0.8 s.

3.2.3. Cutting Entry Region (CER) Analysis

By observing the process of the drilling cuttings entering into the sieve holes in the CFD-DEM simulation, the CER range was obtained. As shown in Figure 12, with the rotation of the SMH drill pipe in the borehole, the drilling cuttings could only enter the sieve holes in a certain area in the circumferential direction of the drill pipe. Figure 12a shows the CER variation with drill pipe rotary speeds of 120, 140, 160, and 180 rpm, and the range of CER at the corresponding rotary speed is indicated in the pie charts A, B, C, and D, respectively. Pie chart E is the superposition of A, B, C, and D. As shown in Figure 12a, the CER shrank with the increase in drill pipe rotary speed, which is consistent with the CER changing, mentioned in Figure 4b. In fact, outside the CER, drilling cuttings at the bottom of the cutting discharge channel in the inner hole of the drill pipe could fall into the sieve holes under the action of gravity. If there is a gap outside the drill pipe, and the rotary centrifugal force on cuttings is greater than the resultant force, the drilling cuttings in the discharge channel will be thrown out through the sieve holes.

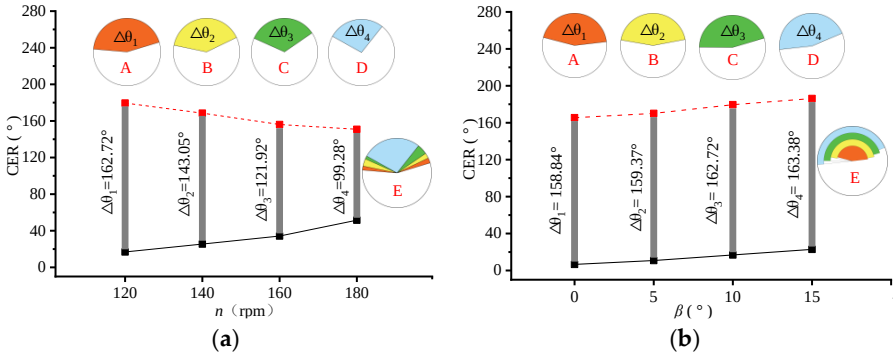

Figure 12. CER variations with n and β. (**a**) Drill pipe rotary speed; (**b**) sieve hole inclination angle.

Figure 12b shows the CER variation at β values of 0°, 5°, 10°, and 15°, and the range of the CER at the corresponding β value is indicated in pie charts A, B, C, and D, respectively. Pie chart E is the superposition of A, B, C, and D. As shown in Figure 12b, the sieve hole inclination angle had little effect on the CER size but led to offset the CER against the drill pipe's rotary direction, which agrees with the CER changing mentioned in Figure 4c.

4. Drilling Cuttings Entering into Sieve Holes in the Laboratory Experiment

4.1. Materials and Methods

4.1.1. Test Equipment

For further illumination of the drilling cuttings' entrance into the sieve holes and the optimization of the SMH drill pipe, an experiment was conducted by using the test equipment shown in Figure 13, which was composed of a fixing frame, rotation motor, frequency converter, air supplier, drilling cutting box, and discharge pipe. The rotation motor was regulated by the frequency converter, whose speed ranged from 0 to 200 rpm. The air supplier was composed of an air source processor and an air compressor with the rated pressure of 0.8 MPa. Moreover, the drilling cutting box was adopted to accommodate drilling cuttings with a length of 300 mm, width of 240 mm, and height of 400 mm. With the aid of pressured air from the air compressor, drill pipe rotation, and gravity, the drilling cuttings were discharged out of the SMH drill pipe and discharge pipe.

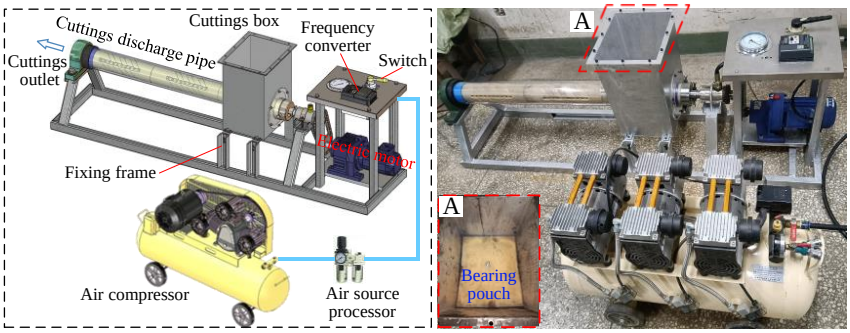

Figure 13. Equipment used in laboratory.

4.1.2. Drilling Cuttings and SMH Drillpipe in Laboratory

The drilling cuttings used in the laboratory were collected from Pingdingshan No. 1 coal mine, whose size distribution is shown in Figure 6c. In the laboratory, the SMH drill pipes were simplified only with a bearing layer that was made of nylon (Figure 14). The diameter of the test SMH drill pipe was 89 mm, the length was 390 mm, and the total number of sieve holes on the SMH drill pipe was 40. As shown in Figure 14, sixteen drill pipes with different D, H, and β were designed and provided by an orthogonal test (L16(4^5)) with five factors, including sieve hole depth (H), sieve hole diameter (D), sieve hole inclination angle (β), drill pipe rotary speed (n), and vertical load (L) on the drilling cuttings in the cutting box. In addition, each factor had four levels in the laboratory, which are listed in Table 2.

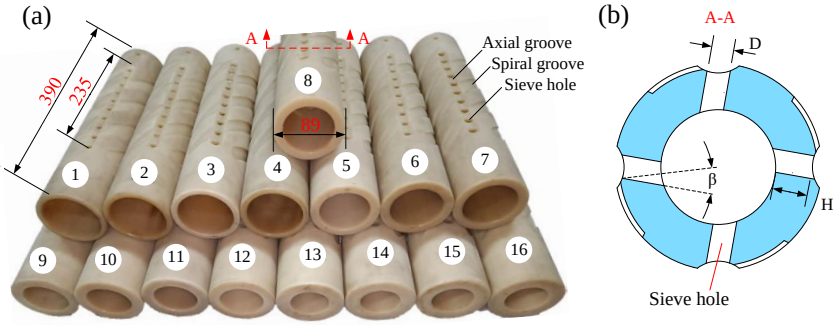

Figure 14. Structure and size of SMH drill pipes for test. (**a**) SMH drill pipe; (**b**) view of cross section.

Table 2. Factors and levels in orthogonal test.

Levels	Factors				
	H **(mm)**	***D*** **(mm)**	***β*** **(°)**	***n*** **(rpm)**	***L*** **(KPa)**
1	4	8	0	100	0
2	8	9	5	120	2
3	12	10	10	140	4
4	16	11	15	160	6

4.1.3. Experimental Procedures

The experimental procedures can be explained as follows:

(1) We placed the SMH drill pipe into the cutting box, which was connected to the rotation motor; (2) we set 20 kg of drilling cuttings into the cutting box, imposed a vertical load on a bearing pouch (as shown in Figure 13) on the drilling cuttings, and then placed the upper cover on the cutting box; (3) we turned on the air compressor with a pressure of 0.4 MPa, set the electric motor speed by a frequency converter, and turned on the rotation motor and switch.

In the laboratory, drilling cuttings were collected from the outlet of the cutting discharge pipe for 60 s. The total mass of the drilling cuttings over those 60 s was measured by a balance. Additionally, we focused on the mass of the drilling cuttings entering into a single sieve hole per minute (MDCS), which was the total discharging cutting mass divided by the number of sieve holes. In order to reduce the possible error, tests under each condition were carried out three times, and the average value was obtained.

4.2. Experimental Results

4.2.1. Influence of Drill Pipe Rotary Speed

Figure 15 shows the variation in the MDCS with the rotary speed of the drill pipe ranging from 100 to 160 rpm. It can be seen that the values of MDCS were 94.5, 96.7, 86.4, and 73.9 g/min at the rotary speed of the drill pipe of 100, 120, 140, and 160 rpm, respectively. This indicates the MDCS increased first and then decreased with the increase in drill pipe rotary speed. Moreover, there was a critical rotary speed for drilling cuttings entering into the sieve holes, which was 120 rpm in this study. At the critical rotary speed, the drilling cuttings entered into the sieve holes at the highest rate. Combined with the analysis in Section 2.2, when the centrifugal force was greater than the weight of the drilling cuttings, the drilling cuttings could not enter into the sieve holes without imposing an external extrusion force on the drilling cuttings.

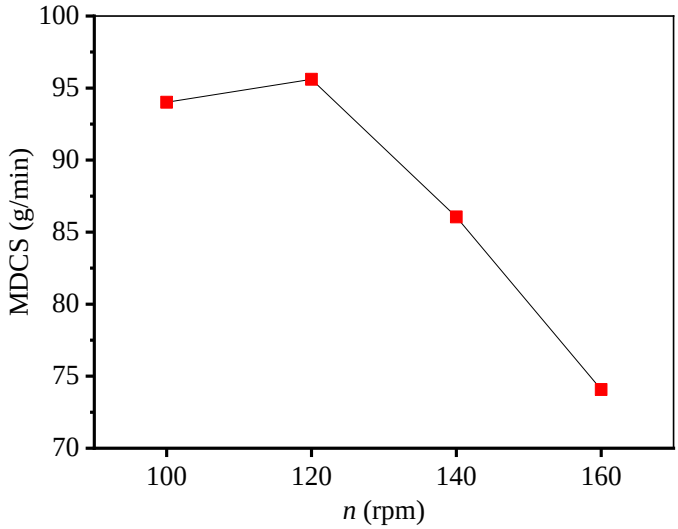

Figure 15. Influence of SMH drill pipe rotary speed on MDCS.

4.2.2. Influences of Sieve Hole Diameter, Inclination Angle, and Depth

The diameter, inclination angle, and depth of the sieve hole set in the SMH drill pipe were critical to the drilling cuttings' entrance into the inner hole of the drill pipe. Figure 16 shows the MDCS variation with the sieve hole diameter (D). It can be seen that the values of MDCS were 56.5, 73.3, 97.2, and 121.5 g/min at the diameters of 8, 9, 10, and 11 mm, respectively, indicating the rising trend of the MDCS with the increase in the sieve hole diameter. The relationship between the MDCS and the sieve hole inclination angle (β) is shown in Figure 16. It can be seen that the values of MDCS were 66.7, 79.6, 97.3, and 106.1 g/min at the inclination angles of 0°, 5°, 10°, and 15°, respectively, indicating the rising trend of the MDCS with the increase in the sieve hole inclination angle. This indicates that when the sieve hole was set as an inclined sieve hole, the MDCS increased. The trend of the MDCS and CER with sieve hole inclination angle was not consistent, as shown in Figures 4c and 16, since the MDCS was not only correlated with the CER but also with the SMH drill pipe rotary speed. Figure 16 shows the MDCS variation with the sieve hole depth (H). It can be seen that the values of MDCS were 118.9, 88.2, 78.6, and 64.1 g/min at the depths of 4, 8, 12, and 16 mm, respectively, indicating that the MDCS negatively correlated with the depth of the sieve hole. The deeper the sieve hole was, the smaller the value of the MDCS was. This is because the deeper the sieve hole, the longer the necessary time for drilling cuttings to enter into the inner hole of the SMH drill pipe via the sieve holes. Moreover, the drilling cuttings entering the sieve holes first rubbed and slid along the sieve hole wall. The lower drilling cuttings in the sieve hole hindered the migration speed of upper drilling cuttings, which easily led to the accumulation and blockage of drilling cuttings in the sieve hole.

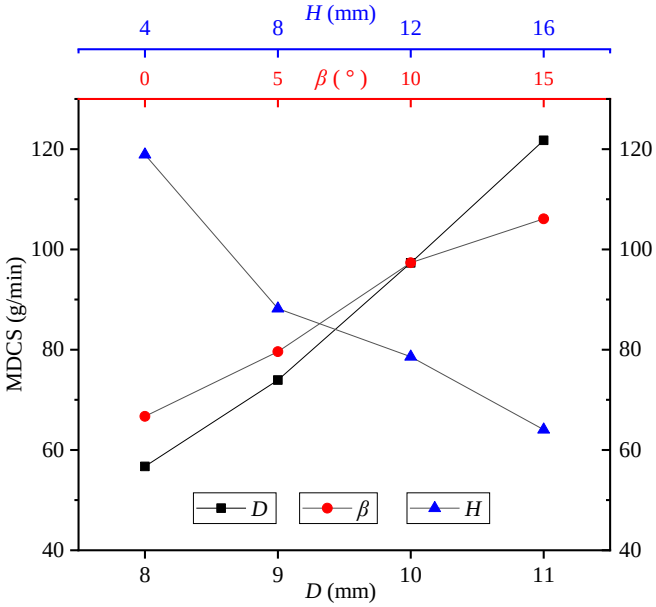

Figure 16. Influence of the sieve hole parameters on the MDCS. Diameter (D); inclination angle (β); and depth (H).

4.2.3. Influence of Vertical Load

Figure 17 shows the variation in MDCS with the vertical load imposed on drilling cuttings in the cutting box through the bearing pouch. This vertical load was not identical to the aforementioned extrusion force in Section 2.2 on drilling cuttings, but they had the same effect on the drilling cuttings entering into the sieve holes. At the vertical loads of 0, 2, 4, 6 KPa, the values of the MDCS were 64.5, 91.2, 95.0 and 98.3 g/min, respectively. This indicates that the greater the vertical load on the drilling cuttings in the cutting box was, the higher the MDCS was. In the actual drilling process, the extrusion force imposed on the drilling cuttings out of the SMH drill pipe is affected by the torque of drill pipe shown in

the drill rig, the stress in the coal/rock around the borehole, the shape of the drill pipe, and the amount of the drilling cuttings outside the SMH drill pipe. The drilling cuttings outside the drill pipe enter into the inner hole via the sieve holes and are discharged outward, which will relieve the force on the drill pipe and reduce the extrusion force on drilling cuttings. Therefore, the extrusion force on the SMH drill pipe is in a dynamic equilibrium state during the drilling process.

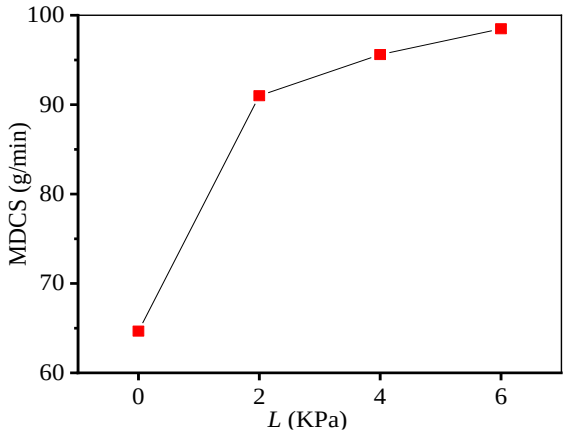

Figure 17. Influence of vertical load on MDCS.

5. SMH Drillpipe Optimization and Trial Manufacture

Through the range analysis of the above orthogonal test data, the influences of different factors on MDCS were obtained. As shown in Figure 18, the sieve holes' diameter and depth were the key factors affecting the drilling cuttings entering into the sieve holes; the influence of the SMH drill pipe's rotary speed on the drilling cuttings entering into the sieve holes was relatively small. Therefore, the preferred sieve hole parameters of the SMH drill pipe were preliminarily determined to be 10 mm (D), 8 mm (H), and 10° (β) considering the drill pipe strength, manufacturing technology, etc.

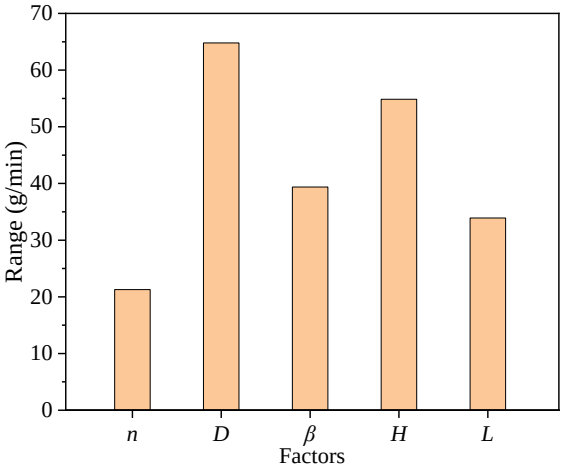

Figure 18. Range analysis of orthogonal test.

The parameters of the sieve hole on the SMH drill pipe affect the strength of the SMH drill pipe. Therefore, numerical simulation on the strength of the SMH drill pipe via the ANSYS15.0 STAIC STRUCTURE component was conducted under the drill rig torque of 7300 N·m and the pulling force of 100 kN [44,45]. The outer diameter of the drill pipe was 89 mm, and the spacing between the sieve holes was 24 mm. The material of the SMH drill pipe was S135-grade steel pipe conforming to API Spec 5DP, and its yield strength is 931~1138 MPa [46,47]. Figure 19a shows the equivalent stress of the SMH drill pipe, and its maximum value was 541.2 MPa. The maximum stress was at the edge of the sieve

hole. Figure 19b shows the equivalent total strain of the drill pipe. It can be seen that the maximum value of the equivalent total strain was 2.7×10^{-3}, where the drill pipe was in the stage of elastic deformation without plastic failure. Figure 19c shows the safety factor of the drill pipe when the yield strength of the drill pipe was 950 MPa. The minimum safety factor of the drill pipe was 1.76, and it met the requirements for engineering applications.

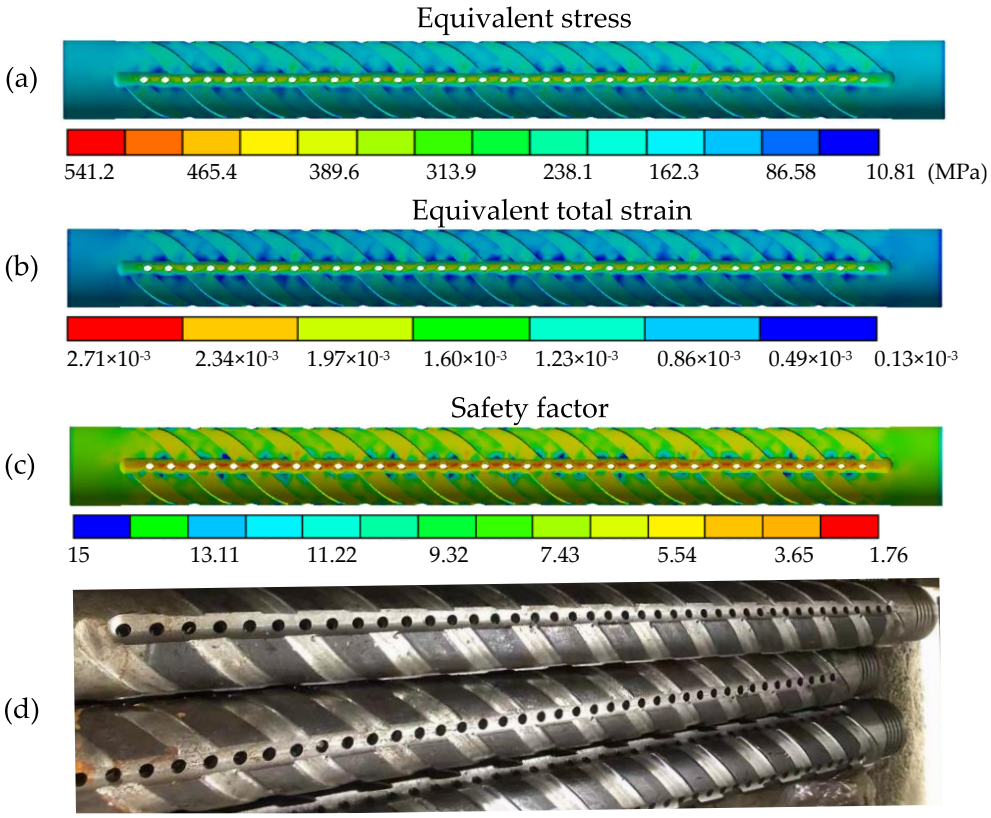

Figure 19. Strength simulation analysis and trial−manufacture of SMH drill pipe. (**a**) Equivalent stress; (**b**) equivalent total strain; (**c**) safety factor; (**d**) SMH drill pipe trial−manufactured.

Based on the influencing factors and strength properties, the SMH drill pipe with a sieve hole diameter of 10 mm, inclination angle of 10°, and depth of 8 mm were determined and trial−manufactured successfully as shown in Figure 19d.

6. Discussion

According to the above analysis and test results, it can be seen that the drilling cuttings out of the SMH drill pipe can enter into the inner hole of the drill pipe via the sieve holes and be discharged out of borehole by air flow, which is different from other researchers' studies on drilling cutting migration with conventional drill pipes [14,27,28,36]. In this paper, the process of drilling cutting in boreholes entering into the inner hole of the SMH drill pipe and its influencing factors were studied, which is beneficial for understanding how the SMH drill pipe works.

The influence of borehole deformation on drilling cuttings' extrusion force and external migration was not considered directly in this study, due to the limitations of the test equipment. Borehole deformation has a time effect, and this is related to in situ stress, gas pressure, coal mechanical properties, and other factors. Borehole deformation is complex, and it can increase the extrusion force on drilling cuttings around the SMH drill pipe, which helps the drilling cuttings enter into the sieve holes, according to the test results. However, borehole deformation would increase the rotating resistance of the drill pipe; so, the SMH drill pipe should be used together with a large torque drill rig, and drilling cuttings in the borehole should be discharged as much as possible before stopping drilling each time.

In addition, the SMH drill pipe's critical rotary speed for drilling cuttings entering into the sieve holes is related to the diameter of the drill pipe. In this study, an SMH drill pipe with a diameter of 89 mm was studied, since this size is commonly used, and its critical rotary speed was about 120 rpm. In future studies, the influences of borehole deformation and different SMH drill pipe diameters should be considered by more functional test equipment and methods.

7. Conclusions

In this paper, an SMH drill pipe used for soft and outburst-prone coal seam was developed, and the influencing factors of drilling cuttings entering into the sieve holes of an SMH drill pipe were analyzed by theory analysis, numerical simulation, and physical experiments. The main conclusions can be drawn as follows:

(1) The SMH drill pipe proposed in this paper was composed of a bearing layer, fluid layer, and anti-sparking layer. Additionally, several sieve holes were set in the SMH pipe. The drilling cutting entering region (CER) of the SMH drill pipe shrank with the rotary speed and expanded with the external extrusion force imposed on the drilling cuttings. Moreover, the position of the CER can be offset with the increase in sieve hole inclination angle.

(2) The drilling cuttings between the borehole wall and SMH drill pipe migrated and accumulated over time and entered into the sieve holes gradually. Spiral and axial grooves on the surface of the SMH drill pipe were beneficial to the drilling cuttings' migration and accumulation. As the drilling cuttings outside the drill pipe accumulated, the compressive force between the drilling cuttings increased, leading to significant increases in the mass and diameter of the drilling cuttings entering into the sieve holes.

(3) By an orthogonal test, the influencing factors of the MDCS included the drill pipe's rotary speed, load imposed, accumulated drilling cuttings, and sieve hole parameters that consisted of depth, diameter, and inclination angle. The sieve hole diameter and depth were the critical factors affecting the MDCS, and an appropriate rotary speed of the drill pipe could attribute to the drilling cuttings entering into the sieve holes. Based on the influencing factors and strength properties, an SMH drill pipe with a sieve hole diameter of 10 mm, inclination angle of 10°, and depth of 8 mm was determined and trial-manufactured.

Author Contributions: Conceptualization, L.D.; methodology, L.D. and Z.W.; validation, W.S.; supervision, Y.S.; writing—original draft preparation, L.D.; investigation, Y.W. All authors have read and agreed to the published version of the manuscript.

Funding: This research was supported by the Postdoctoral Science Foundation of China, grant number 2021M701101; National Natural Science Foundation of China, grant number 41872188; the Science and Technology Project of Henan province, grant number 222102320295; and the Fundamental Research Funds for the Universities of Henan Province, grant number NSFRF220441.

Institutional Review Board Statement: Not applicable.

Informed Consent Statement: Not applicable.

Data Availability Statement: Not applicable.

Conflicts of Interest: The authors declare no conflict of interest.

References

1. Betz, M.R.; Partridge, M.D.; Farren, M.; Lobao, L. Coal mining, economic development, and the natural resources curse. *Energy Econ.* **2015**, *50*, 105–116. [CrossRef]
2. Xie, H.; Wu, L.; Zheng, D. Prediction on the energy consumption and coal demand of China in 2025. *J. China Coal Soc.* **2019**, *44*, 1949–1960.
3. Karacan, C.Ö.; Ruiz, F.A.; Cotè, M.; Phipps, S. Coal mine methane: A review of capture and utilization practices with benefits to mining safety and to greenhouse gas reduction. *Int. J. Coal Geol.* **2011**, *86*, 121–156. [CrossRef]

4. Wang, F.; Ren, T.X.; Hungerford, F.; Tu, S.; Aziz, N. Advanced directional drilling technology for gas drainage and exploration in Australian coal mines. *Procedia Eng.* **2011**, *26*, 25–36. [CrossRef]
5. Wang, Z.; Zhang, S.; Zhang, X.; Li, P.; Li, J. Effect of microstructure and chemical composition of coal on methane adsorption. *J. Nat. Gas Eng.* **2020**, *82*, 103507. [CrossRef]
6. Frank, H.; Ting, R.; Naj, A. Evolution and application of in-seam drilling for gas drainage. *Int. J. Min. Sci. Technol.* **2013**, *23*, 543–553. [CrossRef]
7. Wang, Z.; Sun, Y.; Wang, Y.; Zhang, J.; Sun, Z. A coupled model of air leakage in gas drainage and an active support sealing method for improving drainage performance. *Fuel* **2019**, *237*, 1217–1227. [CrossRef]
8. Flores, R.M.; Wang, G.; Qin, D.; Xi, Y.; Rukstales, L.R. Advancing CMM drainage, quality, and utilization with horizontal directional-drilled boreholes in Duanshi Coal Mine, southern Qinshui Basin, China. *Int. J. Coal. Geol.* **2019**, *209*, 1–13. [CrossRef]
9. Liu, C.; Zhou, F.; Yang, K.; Xiao, X.; Liu, Y. Failure analysis of borehole liners in soft coal seam for gas drainage. *Eng. Fail. Anal.* **2014**, *42*, 274–283. [CrossRef]
10. Wang, Y.; Yu, Z.; Wang, Z. A Mechanical Model of Gas Drainage Borehole Clogging under Confining Pressure and Its Application. *Energies* **2018**, *11*, 2817. [CrossRef]
11. Zhang, X. Mechanical mechanism of spiral drill pipe sticking in soft coal seam. *Geol. Exp.* **1994**, *5*, 71–73.
12. Erge, O.; van Oort, E. Modeling the Effects of Drillstring Eccentricity, Pipe Rotation and Annular Blockage on Cuttings Transport in Deviated Wells. *J. Nat. Gas Sci. Eng.* **2020**, *79*, 103221. [CrossRef]
13. Busch, A.; Johansen, S.T. Cuttings transport: On the effect of drill pipe rotation and lateral motion on the cuttings bed. *J. Pet. Sci. Eng.* **2020**, *191*, 107136. [CrossRef]
14. Ju, G.; Yan, T.; Sun, X. Numerical Simulation of Effective Hole Cleaning by Using an Innovative Elliptical Drillpipe in Horizontal Wellbore. *Energies* **2022**, *15*, 399. [CrossRef]
15. Lu, Y.; Liu, Y.; Li, X.; Kang, Y. A new method of drilling long boreholes in low permeability coal by improving its permeability. *Int. J. Coal Geo.* **2010**, *84*, 94–102. [CrossRef]
16. Liu, C.; Zhou, F.; Kang, J.; Xia, T. Application of a non-linear viscoelastic-plastic rheological model of soft coal on borehole stability. *J. Nat. Gas Sci. Eng.* **2016**, *36*, 1303–1311. [CrossRef]
17. Guo, H.; Lin, F. Study on borehole wall stability of coal seam based on elastic-plastic mechanics analysis. *Min. Saf. Environ. Pro.* **2010**, *37* (Suppl. S1), 106–109.
18. Sun, Y.-N.; Wang, Y.-L.; Di, X.S.; Wang, Z.-F. Analysis on reasons of drilling difficulty in soft and out-burst coal seam. *J. China Coal Soc.* **2012**, *37*, 117–121.
19. Yao, N.; Zhang, J.; Jin, X.; Huang, H. Status and Development of Directional Drilling Technology in Coal Mine. *Procedia Eng.* **2014**, *73*, 289–298. [CrossRef]
20. Shi, Z.; Dong, S.; Yang, J. Key technology of drilling in-seam directional borehole of 3000 m in underground coal mine. *Coal Geol. Explor.* **2019**, *47*, 1–7.
21. Zhang, J.; Wang, Y.; Huang, H. Directional drilling technology and equipment of pneumatic screw motor in soft seam. *Coal Geol. Explor.* **2020**, *48*, 36–41.
22. Li, Q. Research and application of drilling technology combined rotary with direction in soft-fragmentized coal seam. *Coal Sci. Technol.* **2018**, *46*, 101–106. [CrossRef]
23. Mo, H.; Shi, Z.; Hao, S.; Li, Q. Analysis and Application of Treatment Techniques in Horizontal Directional Drilling Borehole Accident. *Procedia Earth Planet. Sci.* **2011**, *3*, 273–279. [CrossRef]
24. Hungerford, F.; Ren, T. Directional drilling in unstable environments. *Int. J. Min. Sci. Technol.* **2014**, *24*, 397–402. [CrossRef]
25. Cui, G. Drill Pipe for Long Hole Drilling with High Gas in Soft Coal Seam. China Patent 255,635,3, 18 June 2003.
26. Wang, Y.; Liu, C.; Sun, Y.; Song, W.; Wang, Z. Numerical simulation of slag discharge principle on prismatic drill pipe in gas extraction drilling hole. *J. Saf. Environ.* **2015**, *15*, 89–93. [CrossRef]
27. Wang, Y.; Yu, Z.; Wang, Z.; Sun, Y.; Lu, B.; Lu, W.; Guo, D. Slag discharge characteristics and engineering application of prismatic grooved drill pipe in borehole collapse. *Arab. J. Geol.* **2022**, *15*, 141. [CrossRef]
28. Yan, T.; Qu, J.; Sun, X.; Chen, Y.; Hu, Q.; Li, W.; Zhang, H. Numerical investigation on horizontal wellbore hole cleaning with a four-lobed drill pipe using CFD-DEM method. *Powder Technol.* **2020**, *375*, 249–261. [CrossRef]
29. Wang, Y.; Zhai, X.; Sun, Y. Reasonable parameters study on grooved drill pipe used in drilling outburst coal seam. *J. China Coal Soc.* **2011**, *36*, 304–307.
30. Jiang, Q.; Du, X.; Zhu, C.; Qi, C.; Huang, F.; Wang, S. Investigation on fluid field characteristics and cinders transport laws in the annulus of grooved drill pipe based on two-phase flow model. *J. Nat. Gas Sci. Eng.* **2021**, *92*, 103972. [CrossRef]
31. Li, D. A new technology for the drilling of long boreholes for gas drainage in a soft coal seam. *J. Pet. Sci. Eng.* **2016**, *137*, 107–112. [CrossRef]
32. Nie, B.; Xue, F. Research progress and development tendency of borehole drilling rod for soft seam. *Coal Sci. Technol.* **2016**, *44*, 47–54.
33. Yao, N.; Yin, X.; Wang, Y.; Wang, L.; Ji, Q. Practice and drilling technology of gas extraction borehole in soft coal seam. *Procedia Earth Planet. Sci.* **2011**, *3*, 53–61. [CrossRef]
34. Wang, Y.L.; Sun, Y.N.; Wang, Z.F.; Song, W.B. Study on the mechanical characteristic of borehole clogging drilling in soft and outburst coal seam. *J. Chin. Coal Soc.* **2015**, *40* (Suppl. S1), 119–125.
35. Zhang, K.; Wang, Z. *Theoretical Mechanics*; Southeast University Press: Nanjing, China, 2017; pp. 104–177.

36. Akhshik, S.; Behzad, M.; Rajabi, M. CFD–DEM approach to investigate the effect of drill pipe rotation on cuttings transport behavior. *J. Pet. Sci. Eng.* **2015**, *127*, 229–244. [CrossRef]
37. Zhang, H.; Zhang, O.; Li, B.; Zhang, J.; Xu, X.; Wei, J. Effect of drill pipe rotation on gas-solid flow characteristics of negative pressure pneumatic conveying using CFD-DEM simulation. *Powder Technol.* **2021**, *387*, 48–60. [CrossRef]
38. Wang, Z.; Hurter, S.; You, Z.; Honari, V.; Sun, Y.; Zhang, S. Influences of negative pressure on air-leakage of coal seam gas extraction: Laboratory and CFD-DEM simulations. *J. Petrol. Sci. Eng.* **2021**, *196*, 107731. [CrossRef]
39. Bekiri, F.; Benchabane, A. Numerical study of drilling fluids flow in drilling operation with pipe rotation. *Mater. Today Proc.* **2022**, *49*, 950–954. [CrossRef]
40. Wei, N.; Liu, Y.; Cui, Z.; Jiang, L.; Sun, W.; Xu, H.; Wang, X.; Qiu, T. The Rule of Carrying Cuttings in Horizontal Well Drilling of Marine Natural Gas Hydrate. *Energies* **2020**, *13*, 1129. [CrossRef]
41. Wu, H.; Zhu, H.-H.; Zhang, C.-C.; Zhou, G.-Y.; Zhu, B.; Zhang, W.; Azarafza, M. Strain integration-based soil shear displacement measurement using high-resolution strain sensing technology. *Measurement* **2020**, *166*, 108210. [CrossRef]
42. Zhang, H.; Zhu, Q.; Gao, B. Optimization of the Structural Parameters and the Teeth Shape of Slip in Drill Rig. *Math. Probl. Eng.* **2021**, *2021*, 9930182. [CrossRef]
43. Wang, G.; Dong, M.; Wang, Z.; Ren, T.; Xu, S. Removing cuttings from inclined and horizontal wells: Numerical analysis of the required drilling fluid rheology and flow rate. *J. Nat. Gas Eng.* **2022**, *102*, 104544. [CrossRef]
44. Liu, Y.; Li, F.; Xu, X.; Yang, B.; Lu, C. Simulation Technology in Failure Analysis of Drill Pipe. *Procedia Eng.* **2011**, *12*, 236–241. [CrossRef]
45. Wu, H.; Wang, S. Finite Element Simulation Analysis of Drill Pipe Based on ANSYS. *Aeronaut. Comput. Tech.* **2010**, *40*, 61–64.
46. Han, Y.; Zhao, X.; Bai, Z.; Yin, C. Failure Analysis on Fracture of a S135 Drill Pipe. *Procedia Mater. Sci.* **2014**, *3*, 447–453. [CrossRef]
47. Yu, Z.; Zeng, D.; Hu, S.; Zhou, X.; Lu, W.; Luo, J.; Fan, Y.; Meng, K. The failure patterns and analysis process of drill pipes in oil and gas well: A case study of fracture S135 drill pipe. *Eng. Fail. Anal.* **2022**, *138*, 106171. [CrossRef]